RNA (1999), *5*:1665–1674. Cambridge University Press. Printed in the USA.

Quantifying the energetic interplay of RNA tertiary and secondary structure interactions

SCOTT K. SILVERMAN,[1] MINXUE ZHENG,[2] MING WU,[2,3] IGNACIO TINOCO, JR.,[2] and THOMAS R. CECH[1]

[1]Howard Hughes Medical Institute, Department of Chemistry and Biochemistry, University of Colorado at Boulder, Boulder, Colorado 80309-0215, USA
[2]Department of Chemistry, University of California, Berkeley and Structural Biology Department, Physical Biosciences Division, Lawrence Berkeley National Laboratory, Berkeley, California 94720-1460, USA

ABSTRACT

To understand the RNA-folding problem, we must know the extent to which RNA structure formation is hierarchical (tertiary folding of preformed secondary structure). Recently, nuclear magnetic resonance (NMR) spectroscopy was used to show that Mg^{2+}-dependent tertiary interactions force secondary structure rearrangement in the 56-nt tP5abc RNA, a truncated subdomain of the *Tetrahymena* group I intron. Here we combine mutagenesis with folding computations, nondenaturing gel electrophoresis, high-resolution NMR spectroscopy, and chemical-modification experiments to probe further the energetic interplay of tertiary and secondary interactions in tP5abc. Point mutations predicted to destabilize the secondary structure of folded tP5abc greatly disrupt its Mg^{2+}-dependent folding, as monitored by nondenaturing gels. Imino proton assignments and sequential NOE walks of the two-dimensional NMR spectrum of one of the tP5abc mutants confirm the predicted secondary structure, which does not change in the presence of Mg^{2+}. In contrast to these data on tP5abc, the same point mutations in the context of the P4–P6 domain (of which P5abc is a subdomain) shift the Mg^{2+} dependence of P4–P6 folding only moderately, and dimethyl sulfate (DMS) modification experiments demonstrate that Mg^{2+} does cause secondary structure rearrangement of the P4–P6 mutants' P5abc subdomains. Our data provide experimental support for two simple conclusions: (1) Even single point mutations at bases involved only in secondary structure can be enough to tip the balance between RNA tertiary and secondary interactions. (2) Domain context must be considered in evaluating the relative importance of tertiary and secondary contributions. This tertiary/secondary interplay is likely relevant to the folding of many large RNA and to bimolecular snRNA–snRNA and snRNA–intron RNA interactions.

Keywords: DMS modification; NMR; nondenaturing gel electrophoresis; P4–P6; P5abc; secondary structure rearrangement; tP5abc

INTRODUCTION

The standard model for RNA folding is hierarchical (Draper, 1992; Westhof & Michel, 1994; Tinoco & Bustamante, 1999). First, secondary structure forms, then tertiary contacts are made using unpaired bases. Recent experiments demonstrate an exception to this general rule. For tP5abc, a truncated 56-nt RNA derived from the P5abc subdomain of the *Tetrahymena* group I intron, nuclear magnetic resonance (NMR) spectroscopy showed that Mg^{2+}-dependent tertiary interactions can force local yet substantial rearrangement of the secondary structure (Wu & Tinoco, 1998). Other examples of such balance between RNA tertiary and secondary structure are known (Gluick & Draper, 1994; Green & Szostak, 1994; Knitt et al., 1994). In general, however, many questions remain about the relative energetic importance of tertiary and secondary interactions in RNA. Here we describe nondenaturing gel electrophoresis, NMR spectroscopy, and chemical-modification experiments designed to examine further the interplay of RNA tertiary and secondary interactions in tP5abc.

By studying two point mutants of tP5abc, U167C and G174A (see Fig. 1), we complement the earlier study by showing that Mg^{2+}-dependent tertiary interactions *cannot* rearrange the tP5abc secondary structure if the secondary structure preference is large enough. The single point mutations are sufficient to alter the balance between tertiary and secondary interactions. We also examine the same two mutations in the intact 160-nt P4–P6 domain, of which P5abc is a subdomain. The

Reprint requests to: Scott K. Silverman or Thomas R. Cech, Department of Chemistry and Biochemistry, Campus Box 215, University of Colorado at Boulder, Boulder, Colordo 80309-0215, USA; e-mail: Scott.Silverman@colorado.edu.
[3]Present address: Bayer Corporation, 4560 Horton Street, Emeryville, California 94608, USA.

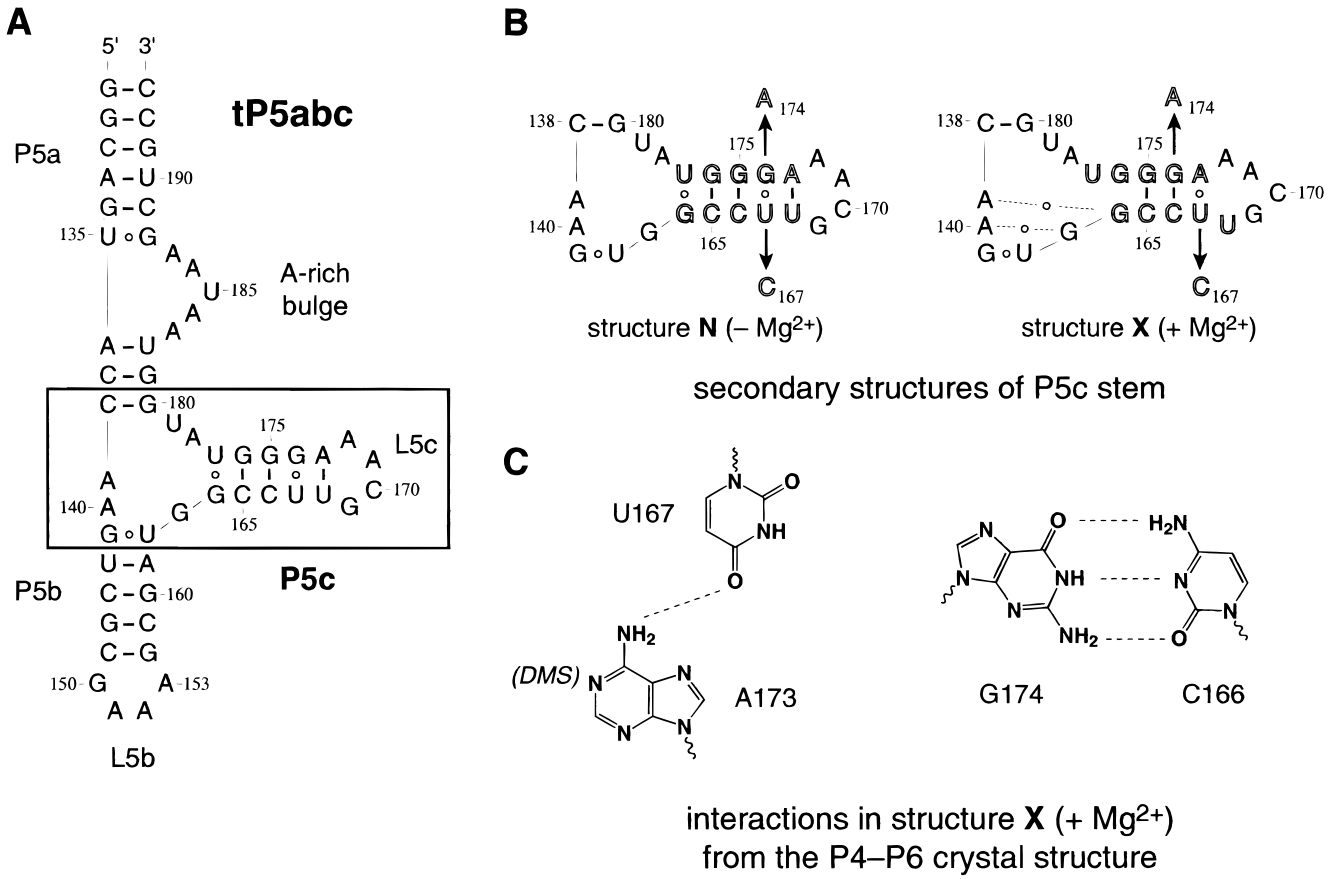

FIGURE 1. Secondary structures of tP5abc. **A**: The structure of isolated tP5abc studied here (Wu & Tinoco, 1998; see Materials and Methods for modifications relative to the wild-type P4–P6 sequence). The P5c stem is boxed; the conventional P4–P6 numbering is used. **B**: The **N** (NMR) and **X** (crystal) secondary structures of the P5c stems. Structure **N** is preferred in the absence of Mg^{2+}, as expected based on the number and type of available base pairs shown in the various structures, and as shown by *mfold* computations. Structure **X** is formed by shifting the upper strand of the P5c stem one step to the left relative to the lower (highlighted bases). The mutations U167C and G174A are indicated. **C**: The U167•A173 and G174•C166 interactions observed in the P4–P6 X-ray crystal structure. Note that the U167•A173 pair is non-Watson–Crick (a single, noncanonical hydrogen bond). The availability of N1 of base A173 to DMS modification is noted. The U167C mutation disrupts the noncanonical U167•A173 hydrogen bond, which should be restored by the compensatory A173G mutation; the G174A mutation disrupts the G174•C166 Watson–Crick base pair, which should be restored by the compensatory C166U mutation.

tertiary interactions in folded tP5abc are a subset of those in fully folded P4–P6 (Murphy & Cech, 1993), so comparison of similar tP5abc and P4–P6 mutants is equivalent to increasing the strength of tertiary interactions that favor a secondary structure rearrangement. We find that for the U167C and G174A mutants, the multiple tertiary interactions in P4–P6 are able to force secondary structure rearrangement of its P5abc subdomain, although the more local subset of tertiary contacts in tP5abc are insufficient. Our results reveal an energetic balance between tertiary and secondary interactions that contribute to the structure of folded RNA molecules.

RESULTS

tP5abc is known to adopt two related secondary structures differing in their P5c stems (Fig. 1). The first structure (**N**) is observed by NMR spectroscopy of tP5abc in the absence of Mg^{2+} (Wu & Tinoco, 1998). The second structure (**X**) is observed with Mg^{2+} in the context of the intact, folded P4–P6 domain by X-ray crystallography (Cate et al., 1996). The trigger for interconverting the **N** and **X** secondary structures is introduction of Mg^{2+}-dependent tertiary interactions. These tertiary contacts stabilize the otherwise disfavored **X** secondary structure, both in tP5abc itself and in the P5abc subdomain of P4–P6.

Mutations in the P5c stem affect tP5abc secondary structure rearrangement

The **N** and **X** secondary structures of tP5abc are related to each other by a one-step change of base-pairing register in the P5c stem (Fig. 1B). By inspection, we identified two point mutations in P5c, U167C and

G174A, each of which should to first order affect **N** only slightly but significantly destabilize **X**. Therefore, these point mutations were predicted to make the **N**-to-**X** secondary structure rearrangement more difficult than for wild-type tP5abc. The U167C mutation was previously found by in vitro selection to accelerate folding of the whole group I intron (Treiber et al., 1998).

Mfold folding computations (Zuker et al., 1999) also predict that U167C and G174A should strongly destabilize the secondary structure of **X** relative to **N**. The computed change in free energy, $\Delta G^{\circ\prime}$ (37 °C), for the transition from the **N** to **X** secondary structure for wild-type tP5abc is +3.4 kcal/mol, whereas for U167C, the gap is +7.8 kcal/mol and for G174A, >+12 kcal/mol (of course, these calculations do not consider tertiary interactions). Because of the noncanonical U167•A173 hydrogen bond in **X** (Fig. 1C), for which *mfold* is not parameterized, the calculations assumed a Watson–Crick base pair between these residues. Nevertheless, the predictions suggest an excellent opportunity to assay the relative importance of RNA tertiary and secondary interactions. Previous work has shown that Mg^{2+}-dependent tertiary interactions can rearrange the wild-type tP5abc secondary structure (Wu & Tinoco, 1998), and we can now test whether Mg^{2+} is able to induce the analogous but energetically more difficult **N**-to-**X** secondary structure rearrangement for the tP5abc U167C and G174A mutants.

By in vitro transcription, we prepared the tP5abc U167C and G174A mutant RNAs. Nondenaturing gels over a wide range of Mg^{2+} concentrations (0 and 0.1–20 mM Mg^{2+}) revealed the relative abilities of the mutants to fold into a compact tertiary structure. As an unfolded control we used tP5abc A186U, previously shown not to fold even at high Mg^{2+} concentrations (Murphy & Cech, 1994; Cate et al., 1997). Wild-type tP5abc undergoes tertiary folding in as little as 0.1 mM Mg^{2+}, which is our estimate for $[Mg^{2+}]_{1/2}$, defined as the Mg^{2+} concentration required to fold half of the molecules. In contrast, folding was severely disrupted in the tP5abc U167C and G174A mutants, which have $[Mg^{2+}]_{1/2} > 20$ mM (Fig. 2A). The greater Mg^{2+} re-

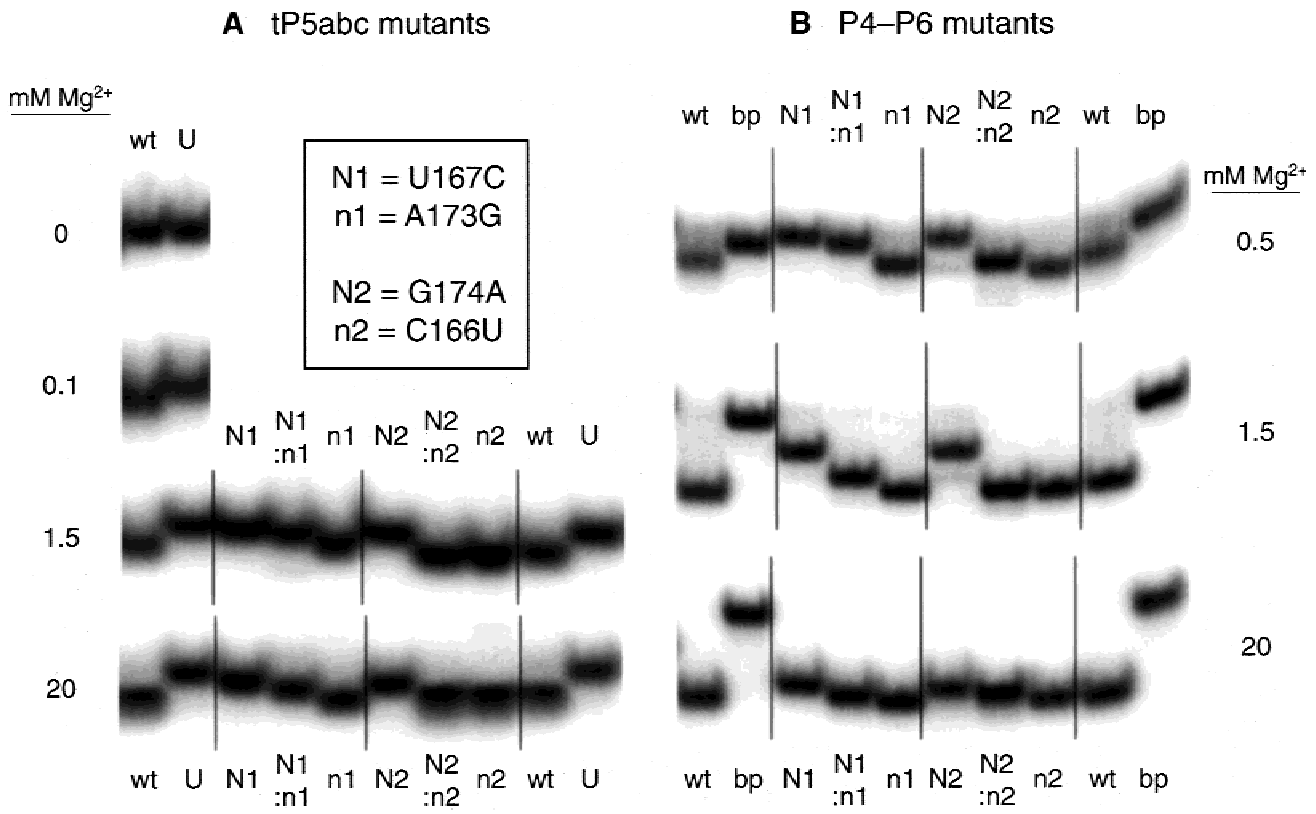

FIGURE 2. Nondenaturing gels of tP5abc and P4–P6 with U167C and G174A mutations. The concentration of Mg^{2+} in the gel and buffer is labeled. **A**: tP5abc mutants. wt: wild-type tP5abc; U: tP5abc A186U unfolded control; N1: U167C; n1: A173G compensatory mutant; N2: G174A; n2: C166U compensatory mutant. Because the A173G (n1) mutation alone disrupts tP5abc folding less than does U167C (N1), the mere presence of a hydrogen bond between these bases is insufficient for proper folding; base identity at U167 is important. Similar relative mobilities for N1 and for N2 were observed at 0.2, 0.5, and 1.0 mM Mg^{2+} (data not shown). At 1.5 mM Mg^{2+}, inclusion of 10 mM Na^{+} in the gel and buffer did not detectably change the relative mobilities (data not shown). **B**: P4–P6 mutants. Sample labeling is the same as in **A**, with bp being P4–P6-bp unfolded control.

quirement is expected if structure **X** is even higher in energy relative to **N** versus wild-type tP5abc, as the folding computations predict.

The nondenaturing gel data allow quantitative estimation of $\Delta\Delta G^{\circ\prime}$, the change in folding free energy of the mutant tP5abc RNAs relative to wild-type tP5abc, as described in Materials and Methods. From the estimated $[Mg^{2+}]_{1/2}$ values, we calculate that $\Delta\Delta G^{\circ\prime} > +6$ kcal/mol for both the tP5abc U167C and G174A mutants. The tP5abc U167C and G174A mutants are clear instances in which RNA tertiary interactions are unable to force secondary structure rearrangement because the secondary structure preference is sufficiently large, in contrast to wild-type tP5abc.

Compensatory mutations restore folding to the tP5abc mutants

To verify that the tP5abc U167C and G174A mutations have the expected structural effects, we examined them in combination with the respective compensatory mutations A173G (which replaces C•A with C•G) and C166U (which replaces A•C with A•U). Note that as a result of the compensatory A173G mutation, the C167•A173 mismatch could be replaced either by a C•G with a single noncanonical hydrogen bond as found in the wild-type U167•A173 interaction in P4–P6 (Fig. 1C), or by a Watson–Crick C167•G173 base pair. We could not distinguish these possibilities with our current NMR data (see below). The A173G mutation was able to partially ameliorate the destabilizing effect of the U167C mutation on folded structure **X** (see N1:n1 in Fig. 2A). The C166U mutation completely overcame the destabilizing effect of the G174A mutation on folded structure **X** (see N2:n2 in Fig. 2A). This suggests that primary effect of each original mutation is indeed disruption of secondary structure interactions, which are restored by the appropriate compensatory mutation, and not disruption of any tertiary contacts.

NMR spectroscopy confirms that tP5abc U167C adopts the N secondary structure and does not rearrange upon Mg^{2+} addition

The secondary structure of the tP5abc U167C mutant in the absence of Mg^{2+} was determined by the sequential NOE connectivity of its imino protons from two-dimensional (2D) NMR spectroscopy (Fig. 3). The NMR-determined secondary structure matches that of structure **N** predicted by the folding computations, as shown by the following observations. The overall chemical shifts and NOE connectivity of the tP5abc U167C imino protons were analogous to those of wild-type tP5abc (Wu & Tinoco, 1998). Alteration of the G174•U167 wobble pair to a G174•C167 Watson–Crick base pair was clearly reflected in the 2D NOESY spectrum: the strong imino-to-imino NOE cross peak from the G174•U167 base pair was absent, and the chemical shift of the G174 imino proton moved from 10.9 ppm (typical for a G•U wobble pair) to 12.9 ppm (typical for a Watson–Crick G•C base pair). Sequential NOE connectivity from the G174 imino proton to the U168 imino proton was observed. Sequential NOE walks could be extended to both U177 and G164 through G176 (Fig. 3B, red lines). Finally, the characteristic G141•U162 and G164•U177 NOE cross peaks were unchanged compared to wild-type tP5abc. As a whole, the NMR data unambiguously show that the tP5abc U167C mutant adopts the **N** secondary structure in the absence of Mg^{2+}.

The 2D NOESY spectrum of tP5abc U167C acquired in the presence of 2 mM Mg^{2+} was essentially unaltered relative to the spectrum obtained in the absence of Mg^{2+} (data not shown). In particular, the NOE cross peak from G174 to U168 and the other characteristic NOE cross peaks described above were still present. This supports the conclusion from the nondenaturing gel data (Fig. 2) that the tP5abc U167C secondary structure does not rearrange upon addition of Mg^{2+}.

The U167C and G174A mutations in the context of P4–P6 have only moderate effects

The tertiary interactions in tP5abc are only a subset of those in the entire P4–P6 domain (Murphy & Cech, 1993), and we next examined the U167C and G174A mutations in P4–P6. Our principal interest was whether the multiple tertiary interactions in P4–P6 are able to force secondary structure rearrangement of the P5abc subdomain, although the subset of such tertiary interactions in isolated tP5abc is insufficient as described above. For P4–P6, the unfolded control is P4–P6 J5/5a-base-paired (P4–P6-bp), which is locked into an extended conformation and cannot undergo the major folding transition that juxtaposes the P5abc and P4 + P6 subdomains of P4–P6 (Murphy & Cech, 1993). Nondenaturing gels (Fig. 2B) showed that the P5c mutations that significantly disrupt tP5abc folding also affect P4–P6 folding, but to a lesser extent. In contrast to the tP5abc mutants, moderate concentrations of Mg^{2+} were able to overcome much of the destabilization for the P4–P6 mutants (Fig. 4). The P4–P6 U167C and G174A mutants each have tertiary folding $[Mg^{2+}]_{1/2} = 1.3$ mM, versus 0.67 mM for wild-type P4–P6. This roughly twofold change in the Mg^{2+} folding requirement translates to a $\Delta\Delta G^{\circ\prime}$ of 1.5–6 kcal/mol, as described in Materials and Methods (the wide spread is due to possible differences in the number of Mg^{2+} ions bound). In contrast, the disruptive P4–P6 A186U mutation led to a very large shift in $[Mg^{2+}]_{1/2}$ (Fig. 4), from which we estimate the corresponding $\Delta\Delta G^{\circ\prime}$ as $\gg +6$ kcal/mol.

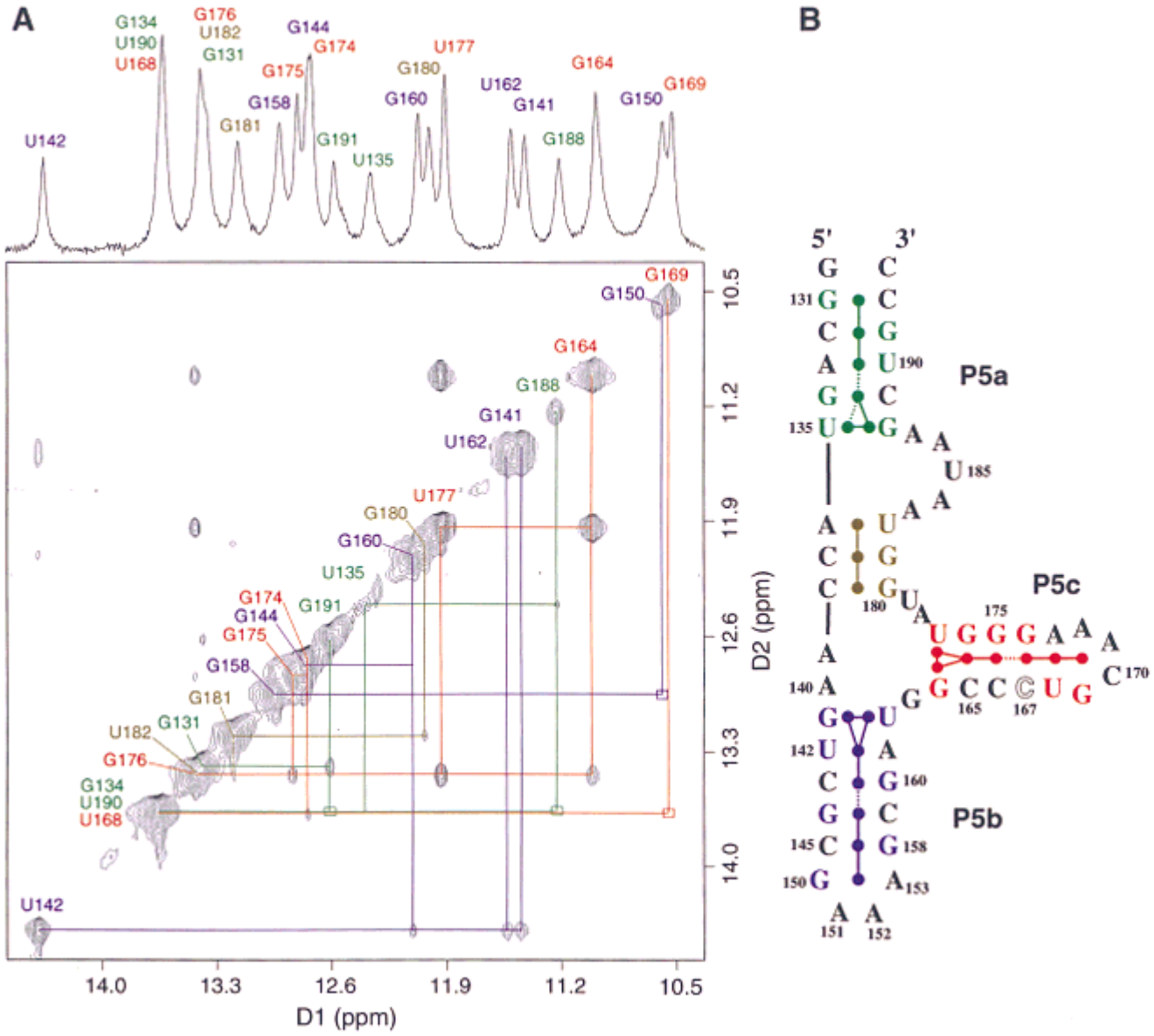

FIGURE 3. Structure of the tP5abc U167C mutant as determined by NMR spectroscopy. **A**: NMR spectra of the tP5abc U167C mutant. Shown are the 1D imino proton spectrum (upper) and the 2D NOESY spectrum (lower). Both spectra were acquired at 10 °C; the NOESY mixing time was 150 ms. A sequential NOE cross peak is joined to two imino proton resonances by a horizontal and a vertical line. The lines are color-coded to match the four stems in **B**. The small square boxes in the 2D spectrum indicate cross peaks that are only visible at a lower contour level. Two sequential NOE cross peaks are absent: G144–G160 and U135–G134. In addition, the sequential NOE cross peaks of G174–G175 and G134–U190 are too close to the strong diagonal peaks to be detected. Despite the missing cross peaks, we are confident of the assignments of these imino protons by comparison to the spectrum of tP5abc, in which the former two analogous cross peaks are extremely weak. For comparison spectra of wild-type tP5abc, see Figure 1 of Wu & Tinoco (1998). **B**: The NMR-determined secondary structure of the tP5abc U167C mutant and its sequential NOE connectivities summarized from the 2D NOESY spectrum in **A**. This secondary structure matches the predicted structure **N** (Fig. 1). The four stems are coded in different colors. The filled colored circles represent observed imino protons. A solid colored line represents an observed NOE connectivity in the corresponding stem, whereas a broken line indicates a missing sequential NOE connectivity.

DMS modification experiments

Large-scale tertiary folding of P4–P6 could occur without proper folding of its P5abc subdomain. Therefore, an important issue for the P4–P6 mutants is whether their P5abc subdomains indeed have a rearranged secondary structure in the presence of Mg^{2+}. To address this, we performed dimethyl sulfate (DMS) modification experiments on wild-type P4–P6 and on the P4–P6 U167C and G174A mutants in the absence and presence of Mg^{2+}. Nucleotide A173 should be inaccessible to DMS when P4–P6 adopts secondary structure **N**, because the base is Watson–Crick paired to U168 (Fig. 1C). However, in structure **X**, N1 of A173 should

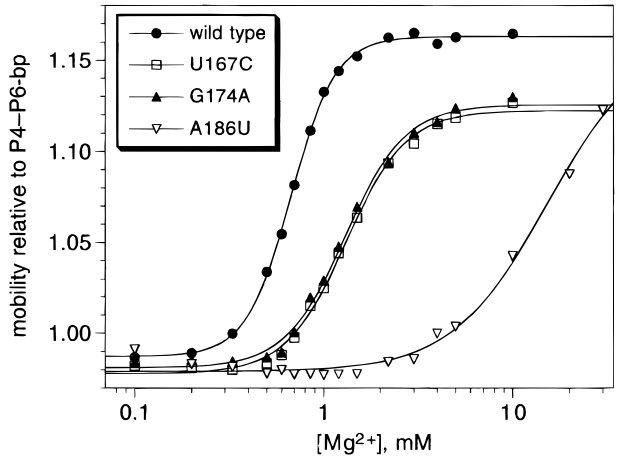

FIGURE 4. Nondenaturing gel Mg^{2+} titration curves. The nondenaturing gel mobility of wild-type P4–P6 and the indicated P4–P6 mutants relative to the unfolded control molecule P4–P6-bp are plotted versus Mg^{2+} concentration, as described elsewhere (Silverman & Cech, 1999). The folding $[Mg^{2+}]_{1/2}$ values for wild-type P4–P6 and for the U167C and G174A mutants were 0.67, 1.31, and 1.30 mM; the fit values of the Mg^{2+} Hill coefficient *n* for these specific experiments were 3.7, 2.8, and 2.8. The $[Mg^{2+}]_{1/2}$ for P4–P6 A186U was 15 mM.

be accessible to DMS, despite a non-Watson–Crick hydrogen bond from A173 to U167. As expected, in wild-type P4–P6 we observe strong DMS modification of A173 only in the presence of 10 mM Mg^{2+} (Fig. 5). Both the U167C and G174A P4–P6 mutants show similar DMS modification at A173 only with Mg^{2+} (Fig. 5), suggesting that their secondary structures rearrange from **N** to **X** with Mg^{2+}. Adjacent base A174 of the G174A mutant also shows modification only in the presence of Mg^{2+}.

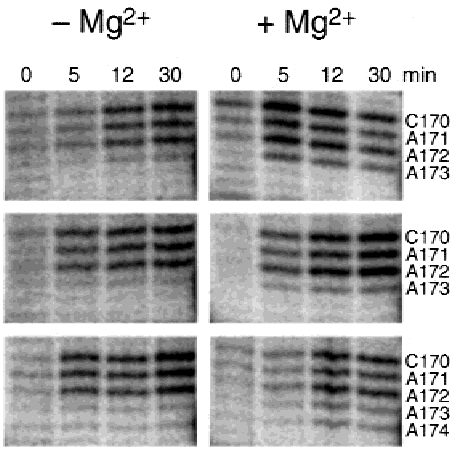

FIGURE 5. DMS modification experiments. Samples of wild-type P4–P6 and the P4–P6 U167C and G174A mutants were exposed to DMS for 0, 5, 12, or 30 min as indicated, in the presence or absence of 10 mM Mg^{2+}, then reverse transcribed using a radiolabeled primer and electrophoresed next to a dideoxy sequencing ladder (not shown). Unpaired nucleotides C170, A171, and A172 of all three P4–P6 constructs are modified by DMS both in the presence and absence of Mg^{2+}. In contrast, base A173 is modified only in the presence of Mg^{2+}, revealing the **N**-to-**X** secondary structure change of Figure 1. For the G174A mutant, base A174 is also modified only in the presence of Mg^{2+}.

DISCUSSION

A complete understanding of RNA folding requires quantitative assessment of the energetic interplay of tertiary and secondary interactions. In this study, we characterize two P5abc mutations to determine the circumstances in which tertiary interactions can rearrange the P5abc secondary structure. By examining both the isolated tP5abc subdomain and the larger P4–P6 domain that contains P5abc, we can control the relative strength of tertiary interactions attempting to force secondary structure rearrangement. From our results we draw simple conclusions about the balance between RNA tertiary and secondary interactions in this system. In particular, we find that a wide range of changes, from mutations at single bases to changes in domain context, can determine whether tertiary contacts are able to rearrange secondary structure. Because short base-paired stem-loops with modest thermodynamic stability are common in natural RNA molecules, the effect seen here—that changing one base in a stem can alter RNA tertiary structure—is likely to be encountered more generally. Furthermore, dynamic snRNA–snRNA and snRNA–intron RNA pairings, which form several base pairs (Burge et al., 1999; Staley & Guthrie, 1999), could in principle affect RNA tertiary structure quite effectively.

Single point mutations disrupt tertiary structure of the isolated tP5abc subdomain

The U167C and G174A mutations were selected for study because the *mfold* computations predict that they should preferentially destabilize the **X** secondary structure (Fig. 1) found in folded P5abc (Cate et al., 1996). Indeed, in tP5abc, these mutations dramatically shift the tertiary folding $[Mg^{2+}]_{1/2}$ from $\sim$0.1 mM to $>$20 mM (Fig. 2A), from which the change in folding $\Delta G^{\circ\prime}$ is computed as $\Delta\Delta G^{\circ\prime} > +6$ kcal/mol. Inasmuch as this energy difference is due to disrupting secondary interactions in **X**, this is consistent with the *mfold* computations, which predict free energy differences of at least several kcal/mol. The NMR experiments (Fig. 3) directly confirm that the secondary structure of tP5abc U167C is unaltered relative to wild-type tP5abc and does not rearrange upon Mg^{2+} addition. The tP5abc U167C and G174A mutants demonstrate that single point mutations can be sufficient to switch a secondary structure from one which is capable of being rearranged by tertiary interactions to one which is locked in and not subject to rearrangement. Thus, while it seems obvious from basic energetic principles that a given set of tertiary interactions will be unable to force secondary structure rearrangement when the secondary structure

preference is sufficiently large, the tP5abc system provides a specific example where point mutations alter the balance of tertiary/secondary structure energetics.

Throughout our analysis, we have made the assumption that point mutations in the P5c stem do not affect tertiary interactions and/or Mg^{2+} binding sites in the folded structure. This is not necessarily true in general. However, the compensatory A173G and C166U mutations restored Mg^{2+}-dependent folding to the U167C and G174A mutants (Fig. 2). These observations, as well as inspection of the P4–P6 crystal structure (Cate et al., 1996), suggest that tertiary contacts and Mg^{2+}–RNA interactions remain undisturbed in the particular mutants we studied.

The U167C and G174A mutations in the P4–P6 domain have lesser effects

In contrast to the results with tP5abc, the same U167C and G174A mutations in the context of the whole P4–P6 domain only shift $[Mg^{2+}]_{1/2}$ twofold, from 0.67 mM to 1.3 mM (Figs. 2B and 4); the $\Delta\Delta G^{\circ\prime}$ is estimated to be in the range of +1.5–6 kcal/mol (see Materials and Methods for explanation of the wide range). We conclude that tP5abc folding is more disrupted by the U167C or G174A mutations than is P4–P6 folding. It is not too surprising that U167C and G174A prevent tP5abc folding, because each disrupts key hydrogen bonds in the P5c stem (Fig. 1). What is perhaps unexpected is that the multiple tertiary interactions in P4–P6 allow folding despite these disruptions. Therefore, we sought to demonstrate that the P5abc subdomains within the P4–P6 mutants indeed undergo the **N**-to-**X** secondary structure rearrangement. Kinetic analysis of ribozyme activity of the P4–P6 mutants in a three-piece assay (Doudna & Cech, 1995) revealed that the U167C and G174A mutations do not destroy catalytic competence (data not shown). However, because the severe A186U mutation did not much disrupt catalysis either, these observations alone do not conclusively demonstrate proper P5abc subdomain folding.

The DMS modification experiments are more decisive. The results show that base A173 of wild-type P4–P6 and of the P4–P6 U167C and G174A mutants is accessible to DMS only in the presence of Mg^{2+} (Fig. 5). This requires some structural transition in which A173 becomes available for reaction with DMS, and the **N**-to-**X** secondary structure rearrangement is the simplest explanation. Therefore, the chemical modification data demonstrate that the P5abc subdomain of the P4–P6 U167C and G174A mutants undergoes secondary structure rearrangement in the presence of Mg^{2+}. We conclude that tertiary interactions present in P4–P6 are capable of forcing secondary structure rearrangement in the mutants, even though the subset of such interactions in context of tP5abc is inadequate to force the same rearrangement. These results show that domain context must also be considered in the balance between tertiary and secondary contributions to RNA structure.

The nondenaturing gel Mg^{2+} titration data (Fig. 4) show that the final, folded state of the P4–P6 U167C and G174A mutants is slightly different than that of wild type. The limiting high-Mg^{2+} mobility of the mutants is lower than that of wild-type P4–P6, suggesting that the mutants have a less compact structure. We also note that base A174 of the G174A mutant is accessible to DMS, despite its location between two hydrogen-bond-associated base pairs. These data suggest that the P5abc subdomains of the U167C and G174A P4–P6 mutants adopt somewhat looser structures than in wild-type P4–P6, which may reflect reduced tertiary interactions between the P5abc and P4 + P6 domains of the molecule. Higher-resolution information, such as that potentially available by NMR spectroscopy, is needed to explore this possibility in more detail.

Energy diagrams to summarize the results

Our results may be understood with the aid of schematic energy diagrams (Fig. 6). The relative free energies of **N** and **X** are depicted according to the experimental data for tP5abc and for P4–P6, for both wild-type and U167C/G174A mutant RNAs. In the absence of Mg^{2+}, the **N** structure is lower in energy than **X** for all sequences studied, as indicated by the *mfold* computations. The energy of **N** is approximately unaffected by U167C or G174A mutation (that is, $\mathbf{N_{wt}}$ and $\mathbf{N_{mut}}$ are essentially isoenergetic). However, the energy of **X** depends strongly on primary sequence ($\mathbf{X_{wt}}$ or $\mathbf{X_{mut}}$). For wild-type tP5abc (Fig. 6A), $\mathbf{X_{wt}}$ is more stable than **N** in the presence of Mg^{2+}. That is, $\Delta G^{\circ\prime}_{wt}$ (the overall folding free energy change) is negative, because tertiary contributions override the secondary structure preference. However, for the tP5abc U167C and G174A mutants, $\mathbf{X_{mut}}$ remains higher in energy than **N** even in the presence of Mg^{2+}. That is, $\Delta G^{\circ\prime}_{mut}$ is positive because the U167C and G174A mutations specifically disrupt secondary interactions in $\mathbf{X_{mut}}$, and tertiary interactions are not strong enough to overcome the secondary structure destabilization.

These data allow us to assign limits to the tertiary folding contributions in tP5abc. The tertiary interactions are worth at least 3.4 kcal/mol, which is the *mfold* value for the secondary structure preference for **N** over **X** in the wild-type sequence, but they are worth less than 7.8 kcal/mol, which is the preference in the U167C mutant.

In the context of the entire P4–P6 domain (Fig. 6B), $\mathbf{X_{wt}}$ and $\mathbf{X_{mut}}$ must both be lower in energy than **N**, because the secondary structure rearrangement occurs upon Mg^{2+} addition even in the U167C and G174A mutants. However, the change in free energy upon Mg^{2+} addition is less favorable for the mutants ($\Delta G^{\circ\prime}_{mut}$ is less negative than $\Delta G^{\circ\prime}_{wt}$). The tertiary interactions are

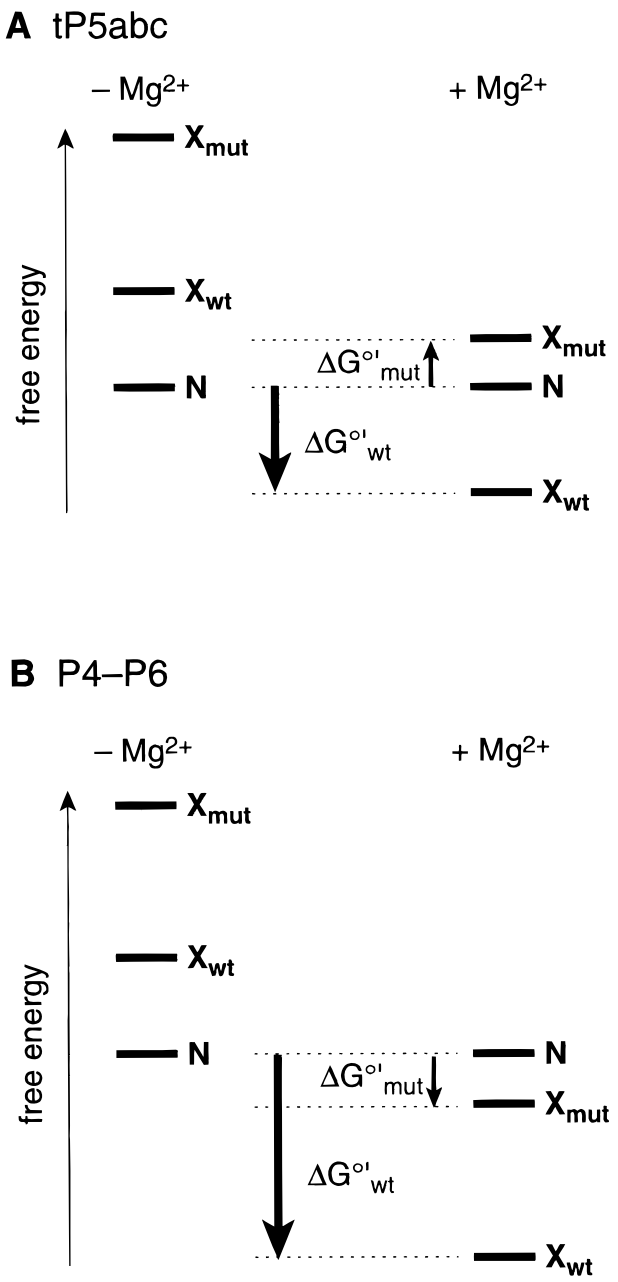

FIGURE 6. Energy diagrams depicting the relationships among the **N** and **X** secondary structures of tP5abc and P4–P6 in the absence and presence of Mg^{2+}. **A**: In the context of the tP5abc subdomain. **B**: In the context of the P4–P6 domain. Only a single species **N** is depicted, because $\mathbf{N}_{wt}$ and $\mathbf{N}_{mut}$ are approximately isoenergetic. In contrast, the energy of the **X** secondary structure depends on the primary sequence ($\mathbf{X}_{wt}$ versus $\mathbf{X}_{mut}$). Arrows depict changes in free energy upon addition of Mg^{2+}, which promotes tertiary structure formation.

larger for P4–P6 compared to tP5abc, and this is enough to force rearrangement from **N** to **X** even with a U167C or G174A mutation.

We note that three assumptions were made in composing Figure 6. First, the energy of **N** is shown as unaffected by Mg^{2+}, which is reasonable to first order because **N** does not incorporate any tertiary contacts. Second, the effects of U167C/G174A on **X** (the difference between $\mathbf{X}_{wt}$ and $\mathbf{X}_{mut}$) are drawn as identical in the absence of Mg^{2+} for both tP5abc and P4–P6. This is justified by previous evidence that neither tP5abc nor P4–P6 undergoes tertiary folding until Mg^{2+} is added. Third, the tertiary contributions upon Mg^{2+} addition are shown as unaffected by the U167C or G174A mutations, which is likely to be an oversimplification, because the stability or rigidity of RNA secondary structure may influence its tertiary structure (Juneau & Cech, 1999; Narlikar et al., 1999). The experimental $\Delta\Delta G^{\circ\prime}$ values calculated from $[Mg^{2+}]_{1/2}$ determinations correspond to the differences between $\Delta G^{\circ\prime}{}_{wt}$ and $\Delta G^{\circ\prime}{}_{mut}$ in each panel, and with the assumptions stated above, the $\Delta\Delta G^{\circ\prime}$s should be identical for tP5abc and P4–P6. However, the experimental data suggest they may in fact differ ($\Delta\Delta G^{\circ\prime} > +6$ kcal/mol for tP5abc versus $+1.5$–6 kcal/mol for P4–P6). Although the assumptions are not strictly correct, the qualitative energetics depicted in Figure 6 are a useful guide to understanding the tertiary and secondary contributions to tP5abc and P4–P6 folding.

CONCLUSIONS

Through analysis of the balance between tertiary and secondary interactions in the structures of tP5abc and P4–P6, we reach two main conclusions. (1) The balance between tertiary and secondary interactions in a natural, folded RNA may be switched by single point mutations at bases involved only in secondary structure. Although RNA tertiary interactions are able to force secondary structure rearrangement of wild-type tP5abc, either point mutation U167C or G174A is sufficient to prevent such rearrangement. (2) Domain context must be considered in evaluating the relative importance of RNA tertiary and secondary interactions. In certain cases, such as the U167C and G174A mutants, multiple tertiary interactions in the P4–P6 domain are able to rearrange the secondary structure of the P5abc subdomain, although the subset of these tertiary contacts in the isolated tP5abc subdomain is insufficient. Because the stabilities of the secondary and tertiary structure elements in the P5abc/P4–P6 system are likely to be typical of many natural RNAs, the balance between secondary and tertiary structure analyzed here is relevant to the folding of many large RNAs and to intermolecular RNA–RNA interactions in the ribosome and spliceosome.

MATERIALS AND METHODS

Cloning, RNA preparation, and radiolabeling

The tP5abc sequence was that previously reported (Wu & Tinoco, 1998), inserted into the pUC19 vector. As before, the sequence is different than that found naturally in P4–P6, as

follows. Bulged base 130 was deleted; base 131 was replaced by G, and complementary base 192 was replaced by C to retain pairing; these changes make the first 2 nt of the sequence GG to allow in vitro T7 transcription. The P5b stem was shortened by 4 bp (bases 144–149 and 154–159 were each replaced by GC); it is unlikely that the shortened P5b stem qualitatively affects the results presented here, for the U167C and G174A mutations are in the relatively remote P5c stem. The wild-type P4–P6 construct was the natural sequence previously reported (Cate et al., 1996) in a plasmid derived from the pTZL-21 construct (Grosshans & Cech, 1991). The J5/5a-base-paired mutant of P4–P6 (P4–P6-bp) was as previously reported (Murphy & Cech, 1993). Mutants were prepared by PCR; DNA fragments were subcloned into pUC19 and verified by automated sequencing over both ligation sites. Plasmids were linearized with *Hin*dIII (P5abc) or *Ear*I (P4–P6). RNA was transcribed in vitro using T7 RNA polymerase prepared by Anne Gooding in the Cech laboratory. Transcription conditions for tP5abc: 15–20 μg/mL linearized plasmid DNA, 40 mM Tris, pH 8.0, 20 mM dithiothreitol (DTT), 20 mM $MgCl_2$, 2 mM each NTP, 2 mM spermidine, 37 °C, 10–20 h. We found that including 100 mM potassium glutamate in the transcription reaction without pH adjustment (Maslank & Martin, 1994) gave about fourfold higher isolated yield of transcription product. RNA was purified by polyacrylamide gel electrophoresis (PAGE), isolated, and quantified as described previously (Silverman & Cech, 1999). Samples for NMR spectroscopy were additionally purified by anion-exchange chromatography (DEAE Bio-Gel agarose, Bio-Rad catalog number 153-0740). For radiolabeling, 25–50 pmol RNA were dephosphorylated (CIP, Boehringer), then incubated with 25 pmol γ-^{32}P-ATP (6,000 Ci/mmol, NEN) and 10 U T4 polynucleotide kinase (New England Biolabs) for 10–30 min, followed by PAGE purification.

Folding computations

The *mfold* program (Mathews et al., 1999; Zuker et al., 1999; accessible online at www.ibc.wustl.edu/~zuker/rna) was used to calculate the relative energies of tP5abc secondary structures. Because little data exist to parameterize *mfold* for such noncanonical interactions as the U167•A173 hydrogen bond in **X** (Fig. 1C), the energy of a standard base pair was used instead. As a consequence, the *mfold* computations are necessarily only a semiquantitative guide to experiments.

Nondenaturing gel electrophoresis and thermodynamic analysis

Gels were prepared, run, and analyzed as described (Silverman & Cech, 1999). All nondenaturing gels were run in 1× TB buffer (89 mM each Tris and boric acid, pH ~8.3) containing Mg^{2+} at the indicated concentration. The tP5abc and P4–P6 RNA sequences can each be characterized by an apparent standard free energy change $\Delta G^{\circ\prime}$ associated with their folding triggered by Mg^{2+}. For any given tP5abc or P4–P6 mutant, we define the folding $\Delta\Delta G^{\circ\prime} = \Delta G^{\circ\prime}(\text{mutant}) - \Delta G^{\circ\prime}(\text{wt})$. The standard free energy of folding for any particular construct is $\Delta G^{\circ\prime} = +n\text{RT}\bullet\ln[Mg^{2+}]_{1/2}$, where $[Mg^{2+}]_{1/2}$ is the concentration of Mg^{2+} necessary for half-folding of the molecule and n is the Mg^{2+} Hill coefficient (see Silverman & Cech, 1999, for a complete discussion of measurements of this type). If n is the same for wild-type and mutant versions of a particular RNA, then $\Delta\Delta G^{\circ\prime} = n\text{RT}\bullet\ln([Mg^{2+}]_{1/2,\text{mut}}/[Mg^{2+}]_{1/2,\text{wt}})$. Note that this analysis is strictly valid only when comparing analogous two-state folding reactions, such as **N** to **X**. In the experiments on tP5abc presented here, this criterion is met, for there is no indication that the P5abc U167C or G174A mutants can access any secondary structure other than **N** or **X**. For folding the entire wild-type P4–P6 domain, the experimental value of n is ~4 (Silverman & Cech, 1999). Because multiple Mg^{2+} ions are observed in the P5abc subdomain in the P4–P6 X-ray crystal structure (Cate et al., 1996), we assume $n = 2$ for P5abc folding. In any case, n is likely <4, because P5abc is a subdomain of P4–P6. We do not feel confident in estimating n directly from the nondenaturing gels, because the absolute difference in gel mobilities at low and high Mg^{2+} concentrations is so small (Fig. 2A).

We compute $\Delta\Delta G^{\circ\prime}$ for the tP5abc U167C and G174A mutants as follows: taking $n = 2$, $[Mg^{2+}]_{1/2,\text{mut}} > 20$ mM, and $[Mg^{2+}]_{1/2,\text{wt}} = 0.1$ mM at 35 °C gives $\Delta\Delta G^{\circ\prime} > +6$ kcal/mol. If the number of Mg^{2+} ions n is greater than 2, the estimate for $\Delta\Delta G^{\circ\prime}$ will increase accordingly. For the P4–P6 U167C and G174A mutants, the determination of $\Delta\Delta G^{\circ\prime}$ is complicated by the observation of different Hill coefficients n for the wild-type and mutant RNAs (Fig. 4). If the value of n is 4 for both the wild-type and the mutants, then applying the equation for $\Delta\Delta G^{\circ\prime}$ given above with $n = 4$, $[Mg^{2+}]_{1/2,\text{mut}} = 1.3$ mM, and $[Mg^{2+}]_{1/2,\text{wt}} = 0.67$ mM at 35 °C gives $\Delta\Delta G^{\circ\prime} = 1.6$ kcal/mol. However, the fit n values for both the P4–P6 U167C and G174A mutants are 2.8. If the value of n is 4 for wild-type but 3 for each mutant, then $\Delta\Delta G^{\circ\prime} = 6.5$ kcal/mol. The correct value of $\Delta\Delta G^{\circ\prime}$ for each mutant probably lies somewhere between these extremes, so we estimate that $\Delta\Delta G^{\circ\prime}$ is between +1.5 and 6 kcal/mol for the P4–P6 U167C and G174A mutants.

NMR spectroscopy

RNA samples were dialyzed extensively (>24 h) against >1 L of buffer (10 mM sodium phosphate, 0.01 mM ethylene diamine tetraacetic acid (EDTA), pH 6.4, in 90% H_2O/10% D_2O). The final RNA concentration in the NMR samples was approximately 2 mM. NMR spectra were acquired on either a 600 MHZ Bruker AMX spectrometer or a 500 MHZ Bruker DRX spectrometer. One-dimensional (1D) and 2D exchangeable imino proton spectra were acquired at 5–20 °C using a 1–1 sequence for water suppression (Plateau & Guéron, 1982; Sklenar & Bax, 1987). The 1D spectra were acquired with 16,384 complex points and processed with a 60° shifted skewed (0.7) sine bell window function. The 2D spectra were acquired with 512 FIDs each containing 2048 complex points and mixing times from 50–250 ms. The 1–1 delay was chosen so that the excitation profile maximized at the imino proton resonances (~12 ppm). Data were processed with FELIX 95 (MSI).

DMS modification experiments

Reaction solutions (249 μL) were prepared with 50 nM P4–P6 RNA, 35 mM Tris, pH 8.0, and 10 mM of either Mg^{2+} or EDTA (for 0 Mg^{2+} conditions). Each solution was annealed at 50 °C for 5 min, then equilibrated at 42 °C for 5 min. After removal of a 50-μL aliquot for a zero time point, 1 μL of a 1:4 dilution of DMS in ethanol was added and the solution was placed at 42 °C. After 5, 12, and 30 min, 50-μL aliquots were removed.

All aliquots were quenched onto 19.5 μL of a quench solution containing 1 μL of 1 mg/mL linear acrylamide, 12.5 μL of 1 M 2-mercaptoethanol, and 6 μL of 3 M NaCl, then precipitated with 250 μL ethanol at -20 °C. The pellets were redissolved in 3.5 μL of 10 mM Tris, pH 8.0. Reverse transcription (RT) was performed by annealing 1 μL of the modified RNA ($\sim$0.7 pmol) with radiolabeled primer ($\sim$2 pmol) in a total volume of 6 μL of 50 mM Tris, pH 8.3, 60 mM NaCl, 10 mM DTT at 90 °C for 2 min, then cooling on ice for $\geq$20 min. The primer was a 21-mer complementary to nt 195–215 of the wild-type P4–P6 sequence. Primer extension was initiated by adding 4 μL of a $MgCl_2$/dNTP/reverse transcriptase stock solution, providing final concentrations of 6 mM Mg^{2+}, 400 μM each dNTP, and 0.4 U/μL AMV reverse transcriptase (Life Sciences). The 10-μL RT reactions were kept at room temperature for 10 min, then 60 °C for 20 min, then placed on ice and quenched with 10 μL stop solution (80% formamide, 1$\times$ TBE, 50 mM EDTA, 0.025% each bromphenol blue and xylene cyanol). Samples were electrophoresed on gels prepared with 10% Long Ranger acrylamide (FMC BioProducts, Rockland, Maine), 8 M urea, 1$\times$ TBE, then dried and exposed to a PhosphorImager screen. Images were scanned and analyzed with ImageQuant 4.0 (Molecular Dynamics).

ACKNOWLEDGMENTS

This work was supported by grants as follows: National Institutes of Health grant GM28039 to T.R.C.; National Institutes of Health grant GM10840, Department of Energy grant DE-FG03-86ER60406, Department of Energy instrumentation grant DE-FG05-86ER75281, and National Science Foundation instrumentation grant DMB 86-09305 to I.T. S.K.S. was supported by an American Cancer Society postdoctoral fellowship and is a fellow of the Helen Hay Whitney Foundation. M.Z. is supported by a Burroughs Wellcome Fund postdoctoral fellowship and is a fellow of the Program of Mathematics and Molecular Biology interface training program. T.R.C. is an Investigator of the Howard Hughes Medical Institute and an American Cancer Society Professor. We thank Evelyn Jabri, Art Zaug, and other members of the Cech laboratory for helpful discussions; Anne Gooding for providing T7 RNA polymerase; Anton McCaffrey for suggesting the use of potassium glutamate to enhance T7 transcription yields; Barbara Dengler for managing the Tinoco laboratory; Jeff Pelton for helpful discussions on NMR; and Dan Herschlag for comments on the manuscript.

Received August 12, 1999; returned for revision September 20, 1999; revised manuscript received September 28, 1999

REFERENCES

Burge CB, Tuschl T, Sharp PA. 1999. Splicing of precursors to mRNAs by the spliceosomes. In: Gesteland RF, Cech TR, Atkins JF, eds. *The RNA World.* 2nd ed. Cold Spring Harbor, New York: Cold Spring Harbor Laboratory Press. pp 525–560.

Cate JH, Gooding AR, Podell E, Zhou K, Golden BL, Kundrot CE, Cech TR, Doudna JA. 1996. Crystal structure of a group I ribozyme domain: Principles of RNA packing. *Science 273*:1678–1685.

Cate JH, Hanna RL, Doudna JA. 1997. A magnesium ion core at the heart of a ribozyme domain. *Nature Struct Biol 4*:553–558.

Doudna JA, Cech TR. 1995. Self-assembly of a group I intron active site from its component tertiary structural domains. *RNA 1*:36–45.

Draper DE. 1992. The RNA-folding problem. *Acc Chem Res 25*:201–207.

Gluick TC, Draper DE. 1994. Thermodynamics of folding a pseudoknotted mRNA Fragment. *J Mol Biol 241*:246–262.

Green R, Szostak JW. 1994. In vitro genetic analysis of the hinge region between helical elements P5-P4-P6 and P7-P3-P8 in the *sunY* group I self-splicing intron. *J Mol Biol 235*:140–155.

Grosshans CA, Cech TR. 1991. A hammerhead ribozyme allows synthesis of a new form of the *Tetrahymena* ribozyme homogeneous in length with a 3′ end blocked for transesterification. *Nucleic Acids Res 19*:3875–3880.

Juneau K, Cech TR. 1999. In vitro selection of RNAs with increased tertiary structure stability. *RNA 5*:1119–1129.

Knitt DS, Narlikar GJ, Herschlag D. 1994. Dissection of the role of the conserved G•U pair in group I RNA self-splicing. *Biochemistry 33*:13864–13879.

Maslank M, Martin CT. 1994. Effects of solution conditions on the steady-state kinetics of initiation of transcription by T7 RNA polymerase. *Biochemistry 33*:6918–6924.

Mathews DH, Sabina J, Zuker M, Turner DH. 1999. Expanded sequence dependence of thermodynamic parameters improves prediction of RNA secondary structure. *J Mol Biol 288*:911–940.

Murphy FL, Cech TR. 1993. An independently folding domain of RNA tertiary structure within the *Tetrahymena* ribozyme. *Biochemistry 32*:5291–5300.

Murphy FL, Cech TR. 1994. GAAA tetralooop and conserved bulge stabilize tertiary structure of a group I intron domain. *J Mol Biol 236*:49–63.

Narlikar GJ, Bartley L, Khosla M, Herschlag D. 1999. Characterization of a local folding event of the *Tetrahymena* group I ribozyme: Effects of oligonucleotide substrate length, pH, and temperature on the two substrate binding steps. *Biochemistry 38*:14192–14204.

Plateau P, Guéron M. 1982. Exchangeable proton NMR without baseline distortion, using new strong-pulse sequences. *J Am Chem Soc 104*:7310–7311.

Silverman SK, Cech TR. 1999. Energetics and cooperativity of tertiary hydrogen bonds in RNA structure. *Biochemistry 38*:8691–8702.

Sklenar V, Bax A. 1987. Spin-echo water suppression for the generation of pure-phase two-dimensional NMR-spectra. *J Magn Reson 74*:469–479.

Staley JP, Guthrie C. 1999. An RNA switch at the 5′ splice site requires ATP and the DEAD box protein Prp28p. *Mol Cell 3*:55–64.

Tinoco I Jr, Bustamante C. 1999. How RNA folds. *J Mol Biol 293*:271–281.

Treiber DK, Rook MS, Zarrinkar PP, Williamson JR. 1998. Kinetic intermediates trapped by native interactions in RNA folding. *Science 279*:1943–1946.

Westhof E, Michel F. 1994. Prediction and experimental investigation of RNA secondary and tertiary foldings. In: Nagai K, Mattaj IW, eds. *RNA–protein interactions.* Oxford, United Kingdom: Oxford University Press. pp 25–51.

Wu M, Tinoco I Jr. 1998. RNA folding causes secondary structure rearrangement. *Proc Natl Acad Sci USA 95*:11555–11560.

Zuker M, Mathews DH, Turner DH. 1999. Algorithms and thermodynamics for RNA secondary structure prediction: A practical guide. In: Barciszewski J, Clark BFC, eds. *RNA biochemistry and biotechnology.* Dordrecht, Netherlands: Kluwer Academic Publishers. pp 11–43.